2022 Second International Conference on Sustainable Mobility Applications, Renewables and Technology (SMART)

Integrated Boost-Converter for 400 V - 800 V Fast-Charging Compatibility

Gabriele Rizzoli
Dept. of Electrical, Electronic and Information Engineering "G. Marconi" University of Bologna
40137 Bologna Italy
Email: gabriele.rizzoli@unibo.it

Michele Mengoni
Dept. of Electrical, Electronic and Information Engineering "G. Marconi" University of Bologna
40137 Bologna Italy
Email: michele.mengoni@unibo.it

Luca Vancini
Dept. of Electrical, Electronic and Information Engineering "G. Marconi" University of Bologna
40137 Bologna Italy
Email: luca.vancini4@unibo.it

Giacomo Sala
Dept. of Electrical, Electronic and Information Engineering "G. Marconi" University of Bologna
40137 Bologna Italy
Email: g.sala@unibo.it

Angelo Tani
Dept. of Electrical, Electronic and Information Engineering "G. Marconi" University of Bologna
40137 Bologna Italy
Email: angelo.tani@unibo.it

Luca Zarri
Dept. of Electrical, Electronic and Information Engineering "G. Marconi" University of Bologna
40137 Bologna Italy
Email: luca.zarri2@unibo.it

***Abstract*—The automotive industry is increasing the voltage of the batteries from 400 V to 800 V to reduce the current rating of the vehicle cabling and the connectors to the external DC fast charger. Although 800 V vehicles are already on the market, the operating charging stations in Europe that support the 800 V charging level are only 1% of the total. Therefore, the electric vehicles must be intrinsically compatible with 400 V DC charging stations with a marginal increase in the cost and the weight of the drive train components. The solution analyzed in this paper reconfigures the electric motor and the three-phase inverter into a multiphase DC/DC boost converter, adapting the battery voltage to the off-board charger. The unconventional use of an electric machine as a coupled inductor requires careful electromagnetic analysis and a dedicated control scheme to control the rotor angular position during the recharge process.**

Keywords— Interior permanent magnet machine; integrated DC/DC battery charger; finite element analysis.

I. Introduction

The range of Battery Electric Vehicles (BEVs) strongly depends on the characteristics of lithium-ion batteries. Nowadays, the energy density of a complete battery pack stands at 200 - 250 Wh/kg [1]. On the other hand, the specific consumption declared on the Worldwide harmonized Light vehicles Test Procedure (WLTP) cycle of most BEVs is 160 - 180 Wh/km [2]. This number is purely an indicator for comparisons among different vehicles because the consumption in actual conditions is significantly higher. Thus, it is evident that one kilogram of battery guarantees a range of about one kilometer. Therefore, the rated range of a BEV is a compromise between battery weight, cost, and vehicle usage. BEVs are best suited for urban areas where the required daily mileage is limited, travel speeds are reduced, and the overnight low-power recharge can restore the battery charge state.

Conversely, private and commercial vehicles intended for long distances in an extra-urban context require batteries of considerable capacity, short recharging time, and recharging facilities distributed throughout the territory. For these reasons, the SAE standard J1772 disciplines the off-board DC charging method for fast charge purposes. Charging times shorter than 30 minutes can only be obtained using high-power off-board chargers (typically from 50 kW up to 350 kW). For these high-power levels, in 400 V BEVs, the charging current can reach 1 kA. Therefore, electrical cables and charging connectors are among the most critical and highly stressed components of the system.

To avoid expensive, bulky, and critical connecting systems, automotive industries are increasing the battery voltage from 400 V to 800 V, even though public infrastructures are not adequate to support 800 V vehicles yet [3]. Although the manufacturers of charging systems are already marketing 800 V solutions, the operating charging stations in Europe that support the 800 V charging level are only 1% of the total [4]. The update of the charging infrastructures cannot be achieved in the short term. There will be a long transition phase in

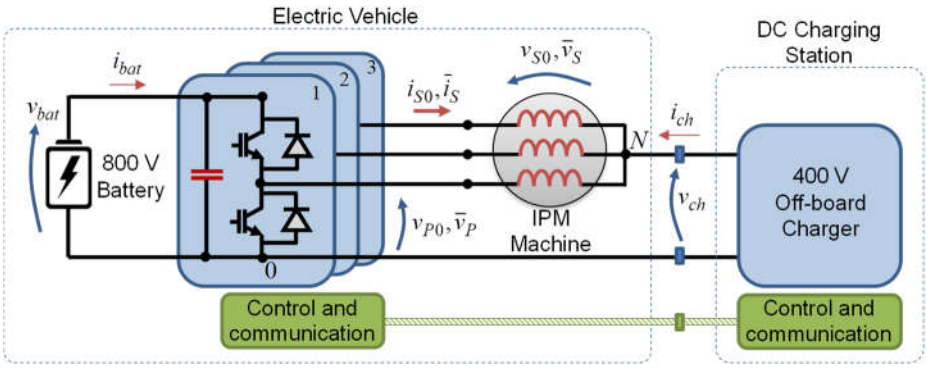

Fig. 1 – Integrated boost charger to achieve compatibility between 800 V-battery vehicles and 400 V fast-charging stations.

which 400 V and 800 V charging centers will coexist. Therefore, new electric vehicles equipped with 800 V batteries must be intrinsically compatible with 400 V DC charging stations. This requirement raises the problem of how to solve the incompatibility between 800 V batteries and 400 V chargers without significantly affecting the cost and weight of the vehicles. The easiest and cheaper solution is to split the 800 V battery pack into two 400 V sub-modules. Thus, each sub-module can be recharged using a 400 V battery charger. However, it is challenging to control and equalize the State of Charge (SOC) of the two sub-modules of the battery. A standard approach is a dedicated onboard DC/DC converter to adapt the battery voltage to the off-board charger [4]. This solution is undoubtedly possible but requires an additional high-power density and low-cost converter, two characteristics that are not easily achievable simultaneously.

A third cost-effective approach for solving the problem is the integrated system illustrated in Fig. 1, which allows the compatibility of an 800 V vehicle with the preexisting 400 V charging infrastructure. The electric drive of the vehicle, consisting of the inverter and the electric motor, is reconfigured into a multiphase DC/DC boost converter, adapting the battery voltage to the off-board charger. The unconventional use of an electric machine as a coupled inductor requires careful electromagnetic analysis and a dedicated control scheme. The current i_{ch} generated by the off-board fast-charger is seen as a common-mode contribution from the point of view of the machine, and a contribution to the electromagnetic torque is generally produced. The torque disturbance might reach high values, which depend on the parameters of the machine and the position of the rotor. Therefore, a control strategy that compensates for the torque unbalance must be implemented to guarantee that, during the recharge process, the torque produced by the electric machine is zero.

This paper focuses on the modeling, control, and current ripple of an integrated battery charger for DC-fast charge using a three-phase Interior Permanent Magnet (IPM) motor as a filter inductance. Several integrated charger solutions have already been published in the literature, but most perform an AC/DC power conversion [5]-[7]. The use of the electric powertrain of the vehicle as an integrated DC/DC boost converter has not been thoroughly investigated.

II. Analytical Model of the System

According to the Vector Space Decomposition (VSD) method, the phase quantities of the machine (voltages, currents, and flux linkages) can be transformed into the homopolar and space vector components by the following symmetrical linear transformations:

$$\bar{y} = \frac{2}{3}(x_A + x_B\bar{\alpha} + x_C\bar{\alpha}^2) \tag{1}$$

$$y_0 = \frac{1}{3}(x_A + x_B + x_C) \tag{2}$$

where $\bar{y}$ and y_0 are the space vector and the homopolar component of three generic time-varying real quantities $x_A, x_B,$ and x_C, and $\bar{\alpha}$ is a unit vector equal to $e^{j2\pi/3}$.

The behavior of an IPM-SM in the fundamental (differential) and third harmonic (homopolar) sub-spaces can be represented through the following set of simplified equations:

$$\bar{v}_S = R_S\bar{i}_S + \frac{d\bar{\varphi}_S}{dt} + j\omega_{me}\bar{\varphi}_S \tag{3}$$

$$\bar{\varphi}_S = L_{Sd}i_{Sd} + jL_{Sq}i_{Sq} + \varphi_{m1} \tag{4}$$

$$v_{S0} = R_S i_{S0} + \frac{d\varphi_{S0}}{dt} \tag{5}$$

$$\varphi_{S0} = L_{S0}i_{S0} + \Re e\left[\varphi_{m3}e^{j3\vartheta_{me}}\right] \tag{6}$$

where $\bar{v}_S$, $\bar{i}_S$, and $\bar{\varphi}_S$ are the space vectors of the stator voltages, currents and flux linkages respectively, and the

scalar quantities v_{S0}, i_{S0}, and φ_{S0} are the homopolar components of the stator voltages, currents, and flux linkages. The parameters of the machine are represented by the direct and quadrature inductances L_{Sd}, L_{Sq}, the homopolar inductance L_{S0}, the resistance of the stator windings R_S, and the magnitudes of fundamental and homopolar fluxes φ_{m1} and φ_{m3} induced in the stator windings by the permanent magnets. The complex equations (3)-(4) are written in a d-q reference frame with the d-axis aligned with the fundamental flux φ_{m1}. This position is identified by the electric angle ϑ_{me}, whose derivative is the electric angular speed ω_{me}. It is worth noting that the homopolar inductance L_{S0} in (6) is assumed constant and independent of the angular position of the rotor because the typical IPM machines used for HEVs/BEVs have a single internal flux barrier (Fig. 3), which exhibits a negligible permeance variation in the homopolar subspace.

The torque generated by the interaction between the stator currents, the rotor reluctance, and the magnetic field of the PM can be derived by analyzing the active power P_{el} absorbed by the machine:

$$P_{el} = \frac{3}{2}\bar{v}_S \cdot \bar{\imath}_S + 3v_{S0}i_{S0}. \tag{7}$$

By introducing (3)-(6) in (7), it can be noted that P_{el} is composed of the Joule loss dissipated on the winding resistance, the variation of the energy stored in the magnetic field, and the mechanical power. The latter term can be used to obtain the analytical expression of the electromagnetic torque generated by the machine, leading to the following expressions:

$$T = T_1 + T_0 \tag{8}$$

$$T_1 = \frac{3}{2}p\left[\left(L_{Sd} - L_{Sq}\right)i_{Sd} + \varphi_{m1}\right]i_{Sq} \tag{9}$$

$$T_0 = -9pi_{S0}\Im m\left[\varphi_{m3}e^{j3\vartheta_{me}}\right]. \tag{10}$$

where p is the number of pole-pairs of the machine. The torque T is composed of the terms T_1 and T_0, which depend on the currents $\bar{\imath}_S$ and i_{S0} respectively. Equation (10) clearly shows that a torque contribution T_0 generated by the homopolar current may arise if the rotor angle ϑ_{me} is different from $k\pi/3$, with k integer. Therefore, a proper current vector $\bar{\imath}_{S1}$ must be injected into the machine to ensure that the total torque at the shaft is zero during the recharge of the vehicle.

To complete the model of the integrated battery charger, the relationship between the motor and the inverter can be derived from Fig. 1 as follows:

$$\bar{v}_S = \bar{v}_P \tag{11}$$

$$v_{S0} = v_{P0} - v_{ch} \tag{12}$$

$$i_{S0} = -\frac{i_{ch}}{3} \tag{13}$$

where v_{P0} and $\bar{v}_P$ are the homopolar and space vector components of the voltages generated by the inverter, v_{ch} and i_{ch} are the voltage and current of the off-board charger.

The instantaneous value of the inverter output power can be used to derive the actual current of the battery i_{bat}. If the power loss of the three-phase inverter is negligible, the input power P_{inv} of the converter can be calculated as follows:

$$P_{inv} \cong \frac{3}{2}\bar{v}_S \cdot \bar{\imath}_S + 3v_{P0}i_{S0}. \tag{14}$$

The instantaneous input power P_{inv} of a three-phase inverter generally consists of a DC contribution and AC terms generated by the switching action (PWM) of the converter. The DC-link capacitor of the converter is designed to absorb the AC contributions of the power. Thus, the actual power provided by the battery pack depends only on the average input power $\hat{P}_{inv}$:

$$P_{bat} = v_{bat}i_{bat} = \hat{P}_{inv}. \tag{15}$$

Equation (15) can be used to calculate the current of the battery pack i_{bat} as follows:

$$i_{bat} = \frac{\hat{P}_{inv}}{v_{bat}}. \tag{16}$$

If the motor is at standstill, the analysis of (15) in steady-state condition allows identifying the control variables that can be employed to regulate the current i_{bat}. By introducing (3)-(6) in (14), and neglecting the Joule loss contributions, i_{bat} can be calculated as follows:

$$i_{bat} = \frac{-3\hat{v}_{P0}i_{ch}}{v_{bat}}. \tag{17}$$

Equation (17) implies that the battery current linearly depends on the current i_{ch} provided by the off-board charger and the homopolar voltage $\hat{v}_{P0}$ imposed by the inverter. These two control variables can be regulated on a different time scale. The voltage $\hat{v}_{P0}$ can be adjusted in every switching period by the inverter control system, while the current i_{ch} is regulated by the off-board charging station. Therefore, the fast control of i_{bat} is achieved by $\hat{v}_{P0}$, while the setpoint for i_{ch} can be updated with a much lower refresh rate.

III. High-Fidelity Model of the IPM Machine

The simulation results presented in the following section V have been obtained considering the High-Fidelity (Hi-Fi) model of the machine illustrated hereafter, which is derived from a Finite Element (FE) mapping of the motor.

A Hi-Fi model of the machine can be obtained by recalling the following generalized voltage equations of the three stator windings A, B, and C:

$$[\boldsymbol{v_{ABC}}] = R_S[\boldsymbol{i_{ABC}}] + \left[\frac{\boldsymbol{d\varphi_{ABC}}}{\boldsymbol{dt}}\right] \tag{18}$$

where:

$$[\boldsymbol{v_{ABC}}] = \begin{bmatrix} v_A \\ v_B \\ v_C \end{bmatrix}, [\boldsymbol{i_{ABC}}] = \begin{bmatrix} i_A \\ i_B \\ i_C \end{bmatrix}, \left[\frac{\boldsymbol{d\varphi_{ABC}}}{\boldsymbol{dt}}\right] = \begin{bmatrix} \frac{d\varphi_A}{dt} \\ \frac{d\varphi_B}{dt} \\ \frac{d\varphi_C}{dt} \end{bmatrix}. \tag{19}$$

In (19), v_A, v_B and v_C are the phase voltages applied to the winding terminals, i_A, i_B and i_C are the phase currents, and φ_A, φ_B and φ_C are the flux linkages.

In an IPM machine with a non-linear iron core, each flux linkage depends on the three phase currents and the rotor angle ϑ_{me}. Thus, the derivative of the flux linkages with respect to time in (19) can be expanded as follows:

$$\frac{d\varphi_A}{dt} = \frac{\partial\varphi_A}{\partial i_A}\frac{di_A}{dt} + \frac{\partial\varphi_A}{\partial i_B}\frac{di_B}{dt} + \frac{\partial\varphi_A}{\partial i_C}\frac{di_C}{dt} + \frac{\partial\varphi_A}{\partial\vartheta_{me}}\frac{d\vartheta_{me}}{dt} \tag{20}$$

$$\frac{d\varphi_B}{dt} = \frac{\partial\varphi_B}{\partial i_A}\frac{di_A}{dt} + \frac{\partial\varphi_B}{\partial i_B}\frac{di_B}{dt} + \frac{\partial\varphi_B}{\partial i_C}\frac{di_C}{dt} + \frac{\partial\varphi_B}{\partial\vartheta_{me}}\frac{d\vartheta_{me}}{dt} \tag{21}$$

$$\frac{d\varphi_C}{dt} = \frac{\partial\varphi_C}{\partial i_A}\frac{di_A}{dt} + \frac{\partial\varphi_C}{\partial i_B}\frac{di_B}{dt} + \frac{\partial\varphi_C}{\partial i_C}\frac{di_C}{dt} + \frac{\partial\varphi_C}{\partial\vartheta_{me}}\frac{d\vartheta_{me}}{dt}. \tag{22}$$

The set of equations (20)-(22) can be expressed in a more compact form by using the following matrix notation:

$$\left[\frac{\boldsymbol{d\varphi_{ABC}}}{\boldsymbol{dt}}\right] = \left[\frac{\boldsymbol{\partial\varphi_{ABC}}}{\boldsymbol{\partial i_{ABC}}}\right]\frac{d}{dt}[\boldsymbol{i_{ABC}}] + \left[\frac{\boldsymbol{\partial\varphi_{ABC}}}{\boldsymbol{\partial\vartheta_{me}}}\right]\frac{d\vartheta_{me}}{dt} \tag{23}$$

where

$$\left[\frac{\boldsymbol{\partial\varphi_{ABC}}}{\boldsymbol{\partial i_{ABC}}}\right] = \begin{bmatrix} \frac{\partial\varphi_A}{\partial i_A} & \frac{\partial\varphi_A}{\partial i_B} & \frac{\partial\varphi_A}{\partial i_C} \\ \frac{\partial\varphi_B}{\partial i_A} & \frac{\partial\varphi_B}{\partial i_B} & \frac{\partial\varphi_B}{\partial i_C} \\ \frac{\partial\varphi_C}{\partial i_A} & \frac{\partial\varphi_C}{\partial i_B} & \frac{\partial\varphi_C}{\partial i_C} \end{bmatrix},$$
$$\left[\frac{\boldsymbol{\partial\varphi_{ABC}}}{\boldsymbol{\partial\vartheta_{me}}}\right] = \begin{bmatrix} \frac{\partial\varphi_A}{\partial\vartheta_{me}} \\ \frac{\partial\varphi_B}{\partial\vartheta_{me}} \\ \frac{\partial\varphi_C}{\partial\vartheta_{me}} \end{bmatrix}. \tag{24}$$

By replacing expression (23) in (18), the dynamic equations that describe the electric behavior of the IPM machine can be obtained:

$$\frac{d}{dt}[\boldsymbol{i_{ABC}}] = \left[\frac{\boldsymbol{\partial\varphi_{ABC}}}{\boldsymbol{\partial i_{ABC}}}\right]^{-1}\left([\boldsymbol{v_{ABC}}] - R_S[\boldsymbol{i_{ABC}}] - \left[\frac{\boldsymbol{\partial\varphi_{ABC}}}{\boldsymbol{\partial\vartheta_{me}}}\right]\frac{d\vartheta_{me}}{dt}\right). \tag{25}$$

Applying a temporal discretization to the dynamic model (25) results in a time discrete representation of the machine that can be numerically integrated and solved using a dedicated simulation software (e.g., MATLAB/Simulink). It is worth noting that the parameters of the model in (24) depend on the rotor angle ϑ_{me} and the instantaneous currents i_A, i_B and i_C. Thus, detailed static FE simulations must be performed to characterize the machine and obtain the flux linkages of the windings for all combinations of the parameters [i_A, i_B, i_C, ϑ_{me}]. Once the flux maps have been obtained, the derivative terms in (24) can be numerically calculated in any operating condition.

Lastly, the FE simulation provides also the electromagnetic torque generated by the machine as a function of [i_A, i_B, i_C, ϑ_{me}]. Thus, the accurate prediction of the torque at the motor shaft can be included in the machine model.

The method presented in this section allows using a Hi-Fi model of the machine for the analysis of the integrated battery charger, avoiding time-consuming FE co-simulations. The accuracy of this model depends on the number of operating conditions used to characterize the machine. If the machine is correctly mapped, the accuracy of the results is significantly higher than that achievable using the analytical model described in Section II.

IV. Control Scheme

The proposed control scheme for the integrated boost converter is shown in Fig. 2. The control algorithm aims to adjust the actual battery current and ensure that the angular position of the motor is kept at its initial value. It can be noted that the scheme includes a communication interface between the onboard boost converter and the off-board charger. SAE J1772-compliant DC fast chargers are designed to be directly connected to the terminals of the vehicle battery. Thus, the off-board charger behaves as a current source that receives the operating setpoint $i_{ch,ref}$ from the Battery Management System (BMS) of the vehicle through a standard communication protocol. The BMS of the vehicle adapts the setpoint of the battery current according to the battery charging strategy, which in most cases is a constant-

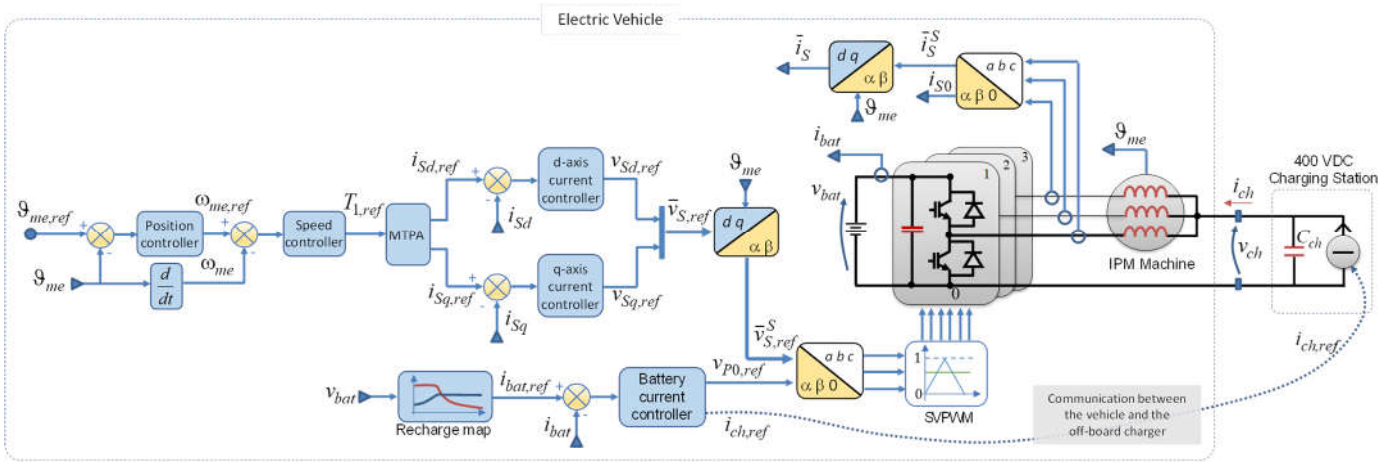

Fig. 2 – Control scheme of the integrated boost converter.

current constant-voltage (CC-CV) profile. Therefore, i_{bat} can be controlled through two degrees of freedom, i.e., the setpoint $i_{ch,ref}$ of the off-board fast charger, and the homopolar voltage $v_{P0,ref}$ imposed by the traction inverter. The selection of these two variables affects the ripple of the phase current, the system efficiency, and the accuracy and control bandwidth of the recharge process.

Equation (10) shows that the homopolar current i_{S0} can generally produce a torque contribution that depends on the angle ϑ_{me} of the machine. To prevent the electric vehicle from moving during the recharge process, a cascaded control loop for the regulation of the angular position of the machine is implemented, as shown in Fig. 2. At the beginning of the charging process, the angle of the machine is sampled and used as a reference. The error between $\vartheta_{me,ref}$ and the actual angle ϑ_{me} is regulated by a position controller, which sets the reference speed $\omega_{me,ref}$. The speed error is then controlled by the speed regulator by acting on the torque reference $T_{1,ref}$. The Maximum Torque per Ampere (MTPA) map of the machine is used to calculate the reference currents $i_{d,ref}$ and $i_{q,ref}$ as a function of the torque reference $T_{1,ref}$, and a pair of PI current controllers generate the required machine voltages $v_{d,ref}$ and $v_{q,ref}$.

Finally, the reference pole voltages $v_{A0,ref}$, $v_{B0,ref}$, and $v_{C0,ref}$ of the inverter are obtained by means of the inverse Park and Clarke transformations. The PWM modulators then synthesize the gate signals for the transistors of the inverter.

V. Simulation Results

Simulations have been performed to verify the effectiveness of the proposed integrated battery charger. The dynamic equations of the system presented in Sections II and III, and the control scheme illustrated in Section IV have been implemented in MATLAB/Simulink. Moreover, FE simulations have been carried out to map the motor and obtain the parameters of the Hi-Fi machine model.

Figure 3 shows the cross section of the 800 V IPM motor considered in this analysis. The rated power of the machine is 100 kW at 6000 rpm, and its main characteristics are reported in Tab. I. The equivalent parameters of the machine model (3)-(6), derived by FE simulations, are listed in Tab. II.

To complete the description of the recharging system, the main parameters of the battery, the three-phase inverter, the external fast charging station, and the vehicle are listed in Tab. III.

In the following, the peculiarities of the IPM machine used as a boost inductance and the operating waveforms of the integrated battery charger are introduced and discussed extensively.

The effectiveness of the algorithm for the active position control of the rotor angle is shown in Fig.4. The figure reports the waveforms of the main system variables at the

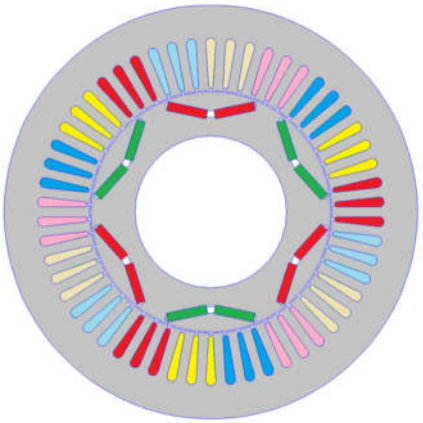

Fig. 3 – Cross section of the 6-pole IPM synchronous machine considered in the simulation analysis.

TABLE I
MAIN PHYSICAL PARAMETERS OF THE IPM MACHINE

Axial length L	150 mm
Outer diameter of the stator	205 mm
Inner diameter of the stator	120 mm
Inner diameter of the rotor	70 mm
Airgap thickness	0.6 mm
Number of stator slots	54
Number of pole pairs	3
Slots per pole per phase	3
Number of conductors per slot	3
Magnet thickness	4.3 mm
Magnet width	23.3 mm
Magnets V-angle	156 mech. deg.
Flux barriers pitch	147.3 el. deg
Electrical steel grade	M250-35A
Permanent magnets grade	NdFeB N35-UH

TABLE II
ELECTRIC PARAMETERS OF THE IPM MACHINE

$R_S = 17.5\ m\Omega$	$\varphi_{m1} = 169$ mWb	$\varphi_{m3} = 8.9$ mWb
$L_{Sd} = 600$ µH	$L_{Sq} = 1980$ µH	$L_0 = 290$ µH

beginning of the recharge process when the battery voltage is 800 V, and the homopolar voltage $v_{P0,ref}$ imposed by the inverter is equal to 400 V. The initial angular position ϑ_{me} of the rotor is $\pi/6$, which corresponds to the condition where the homopolar torque contribution peaks, owing to (10).

At time t_0, the external fast charger increases i_{ch} up to the reference value of 250 A, which corresponds to a power of nearly 100 kW. This results in a homopolar current component i_0 in the stator windings and the generation of a torque contribution T_0, as described in (8)-(10). It can be noted that, as soon as the angle ϑ_{me} varies, the position control loop reacts by injecting the current components i_{Sd} and i_{Sq} in the machine, generating a torque component T_1 that keeps the rotor at its initial position of 30°. The simultaneous circulation of $\bar{\imath}_S$ and i_{S0} leads to different phase currents i_A, i_B and i_C.

At time t_1, the rotor position control loop is deactivated ($i_{d,ref} = i_{q,ref} = 0$). Thus, i_{ch} is equally shared among the machine windings, generating only a homopolar current contribution equal to -83.3 A. The homopolar torque contribution T_0 moves the rotor up to the closest stable angular position at $\vartheta_{me} = \pi/3$ where the total torque is zeroed. The peak of the torque reached in the simulation is 20 Nm, which corresponds to 12.5 % of the motor rated torque. The torque generated during the orientation of the rotor depends on the charge current i_{ch}, the specific machine parameters, the inertia of the load, and the initial position of the rotor.

Fig. 5 illustrates the main waveforms of the system in steady-state condition when i_{ch} is 150 A and $v_{P0,ref}$ is

TABLE III
PARAMETERS OF THE BATTERY, INVERTER, FAST CHARGER, AND VEHICLE

Number of series connected Li-Ion cells	198
Switching frequency of the inverter	30 kHz
Equivalent output capacitance of the fast charger	560 µF
Output current slew rate of the fast charger	500 A/s
Curb weight of the vehicle	2000 kg
Gear ratio of the transmission	5: 1
External radius of the tires	317 mm
Damping coefficient of the vehicle at low speed (proportional to the linear speed)	1800 N s/m

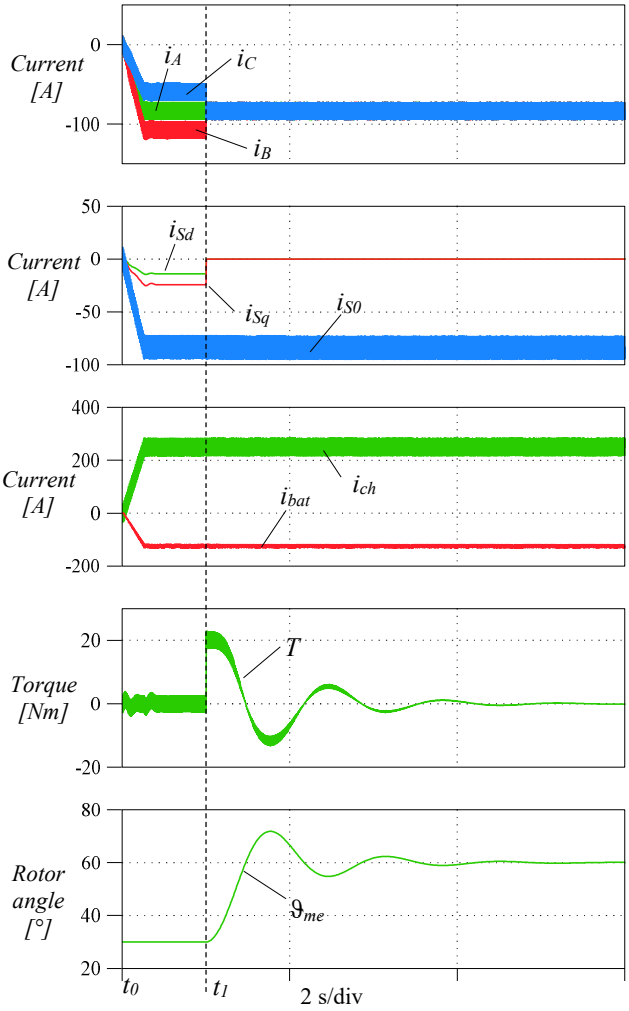

Fig. 4 – Charging process with ($t_0 < t < t_1$) and without ($t > t_1$) the active position control of the rotor angle.

400 V. The figure shows the pole voltages applied by the inverter, the d-q-0 components of the machine stator voltages, the phase currents and their associated d-q-0 components, the current supplied by the fast-charger, and the battery current. In this simulation, the control of the rotor angle is active, so i_{Sd} and i_{Sq} are different from zero. The figure clearly shows that the phase currents are

affected by a relevant current ripple, which is introduced by the homopolar current contribution i_{S0}. This behaviour is caused by the PWM strategy of the inverter. The standard modulating technique used in three phase inverters is based on the comparison between the modulating indexes of the inverter legs with three aligned triangular carriers at frequency F_{sw}. As can be seen in figure, this method is highly effective in the generation of a voltage vector $\bar{v}_S$ with low harmonic content, while the homopolar voltage v_{S0} is essentially a square wave with magnitude $E_{DC}/2$ and frequency F_{sw}. Thus, the ripple of the current i_{S0} is significant and limited only by the inductance L_{S0} of the machine. In addition, the ripple content of i_{S0} is reflected in the current i_{ch} supplied by the external fast charger.

To reduce the current ripple, an additional inductor can be inserted in series with the battery charger. However, this solution requires a bulky inductor (rated for the current i_{ch}) that increases the cost and weight of the system.

A more effective method for the reduction of the homopolar current ripple is the interleaved PWM modulation of the inverter legs. Fig. 6 show the steady state waveforms of the system in the same operating conditions illustrated in Fig. 5 when the carriers of the three PWM modulators are shifted by $T_{sw}/3$. It can be clearly noted that the homopolar voltage v_{S0} is still a square wave but with lower magnitude and frequency equal to $3F_{sw}$. This results in a significant reduction in the ripple of i_{S0} and i_{ch}. However, the side effect of the interleaved technique is the generation of high frequency v_{Sd} and v_{Sq} components. The resulting voltage vector $\bar{v}_S$ shows a considerable magnitude and rotates at angular frequency $2\pi F_{sw}$ in the d-q reference frame, leading to i_{Sd} and i_{Sq} current ripple. It is worth noting that the ripple

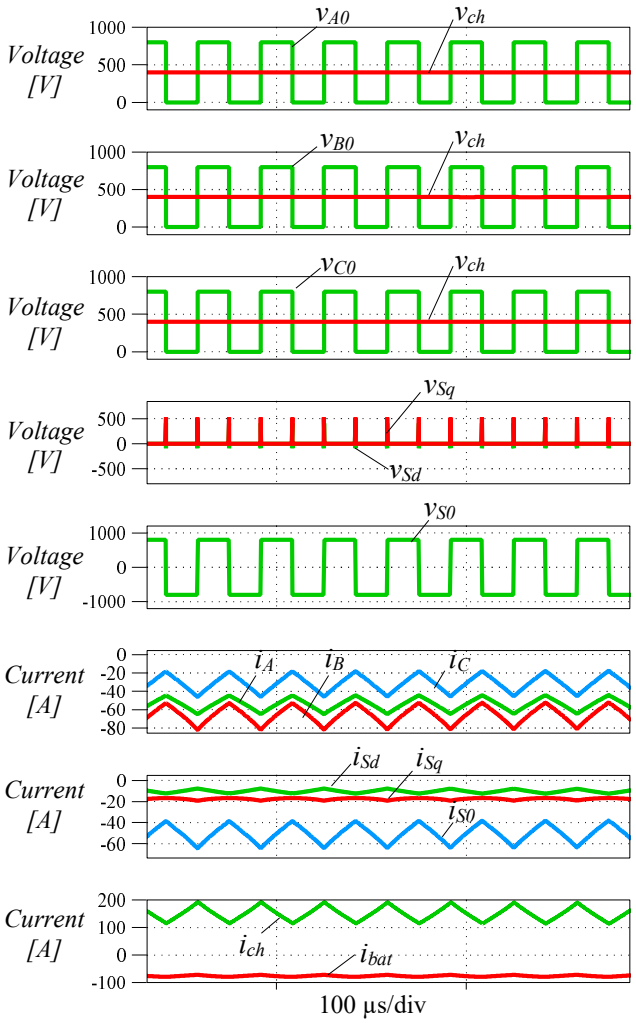

Fig. 5 – Main waveforms of the system in steady state condition when i_{ch} is 150 A, $v_{P0,ref}$ is 400 V, and the standard PWM modulation is implemented.

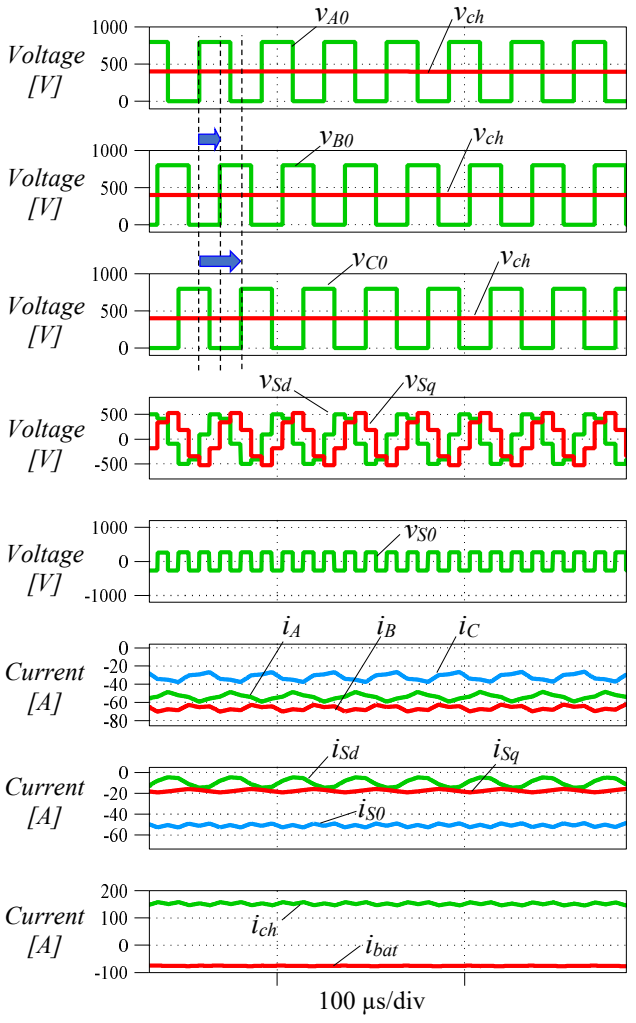

Fig. 6 – Main waveforms of the system in steady state condition when i_{ch} is 150 A, $v_{P0,ref}$ is 400 V, and the interleaved PWM modulation is implemented.

of i_{Sd} is larger than that of i_{Sq}. This behavior can be explained by combining (3) and (4) in the Laplace domain when the angular speed ω_{me} is zero:

$$i_{Sd} = \frac{1}{R_S} \frac{v_{Sd}}{1 + \frac{L_{Sd}}{R_S} s} \tag{25}$$

$$i_{Sq} = \frac{1}{R_S} \frac{v_{Sq}}{1 + \frac{L_{Sq}}{R_S} s}. \tag{26}$$

Transfer functions (25) and (26) show that the filtering action on the current ripple depend on L_{Sd} and L_{Sq}. In IPM machines L_{Sd} is lower than L_{Sq}. Thus, the ripple of i_d is larger than that of i_q even though v_d and v_q in Fig. 6 have the same magnitude and frequency.
Nevertheless, it is evident by comparing Figs. 5 and 6 that the interleaving technique effectively improves the quality of the phase currents of the machine, the fast-charger, and the battery.

VI. CONCLUSION

Automotive industries are increasing the battery voltage from 400 V to 800 V to limit the current level in critical connecting components and cables. However, most of the fast-charging facilities on the territory are compatible only with 400 V batteries and are not yet adequate to support the 800 V level. This paper shows that the electric drive of the vehicle can be used as an interleaved boost converter to step up the 400V generated by the fast charger to the high voltage battery. The recharging current is seen as a homopolar current contribution from the machine point of view. Thus, during the recharge process, a relevant torque contribution applied to the shaft can make the vehicle move. To actively control the rotor angle, a position control loop that adjusts the current vector $\bar{\imath}_S$ has been implemented. Furthermore, to accurately model the behavior of the machine when the current vector $\bar{\imath}_S$ and the component i_{S0} circulate simultaneously in the windings, a Hi-Fi model of the machine has been developed.

ACKNOWLEDGEMENT.

The authors acknowledge Marelli Europe for first bringing the problem to the authors' attention and for the provided insight and expertise that greatly assisted the research.

REFERENCES

[1] M. A. Hannan, M. M. Hoque, A. Hussain, Y. Yusof and P. J. Ker, "State-of-the-Art and Energy Management System of Lithium-Ion Batteries in Electric Vehicle Applications: Issues and Recommendations," in IEEE Access, vol. 6, pp. 19362-19378, 2018.

[2] https://ev-database.org/cheatsheet/energy-consumption-electric-car.

[3] S. Rivera, S. Kouro, S. Vazquez, S. M. Goetz, R. Lizana and E. Romero-Cadaval, "Electric Vehicle Charging Infrastructure: From Grid to Battery," in IEEE Industrial Electronics Magazine, vol. 15, no. 2, pp. 37-51, June 2021.

[4] H. Muhedinovic, "DC Charging compatibility - Grappling with challenges between 800V and 400V", SAE World Congress Experience, Detroit, Michigan, April 5-7, 2022.

[5] G. Pellegrino, E. Armando and P. Guglielmi, "An Integral Battery Charger With Power Factor Correction for Electric Scooter," in IEEE Transactions on Power Electronics, vol. 25, no. 3, pp. 751-759, March 2010.

[6] C. Shi, Y. Tang and A. Khaligh, "A Single-Phase Integrated Onboard Battery Charger Using Propulsion System for Plug-in Electric Vehicles," in IEEE Transactions on Vehicular Technology, vol. 66, no. 12, pp. 10899-10910, Dec. 2017.

[7] S. Foti, A. Testa, G. Scelba, S. De Caro and L. D. Tornello, "A V2G Integrated Battery Charger Based on an Open-End Winding Multilevel Configuration," in IEEE Open Journal of Industry Applications, vol. 1, pp. 216-226, 2020.